Journal of Nuclear Materials 494 (2017) 294–302

Contents lists available at ScienceDirect

Journal of Nuclear Materials

journal homepage: www.elsevier.com/locate/jnucmat

Evaluation of defect formation in helium irradiated Y_2O_3 doped W-Ti alloys by positron annihilation and nanoindentation

Asta Richter [a, *], Wolfgang Anwand [b], Chun-Liang Chen [c], Roman Böttger [d]

[a] Department Engineering Physics, Technical University of Applied Sciences Wildau, Hochschulring 1, 15745 Wildau, Germany
[b] Institute of Radiation Physics, Helmholtz-Zentrum Dresden-Rossendorf, Bautzner Landstr. 400, 01328 Dresden, Germany
[c] Department of Materials Science and Engineering, National Dong Hwa University, Hualien 97401, Taiwan
[d] Institute of Ion Beam Physics and Materials Research, Helmholtz-Zentrum Dresden-Rossendorf, Bautzner Landstr. 400, 01328 Dresden, Germany

HIGHLIGHTS

- All W-Ti-ODS alloys contain less and smaller open volume defects compared to pure tungsten after He irradiation.
- Small defects with high helium-to-vacancy ratio are generated for room temperature irradiation.
- Distinguished He_nV_m-ODS defects are observed for implantation at 600 °C, which are correlated with the pinning to the Y-Ti-O nanoparticles.
- Implantation hardening is observed by nanoindendation and related to microstructural changes analyzed by positron annihilation.

ARTICLE INFO

Article history:
Received 2 April 2017
Received in revised form
5 July 2017
Accepted 20 July 2017
Available online 29 July 2017

Keywords:
W-Ti-ODS alloys
He implantation
Positron annihilation spectroscopy
Nanoindentation
Vacancy defects

ABSTRACT

Helium implanted tungsten-titanium ODS alloys are investigated using positron annihilation spectroscopy and nanoindentation. Titanium reduces the brittleness of the tungsten alloy, which is manufactured by mechanical alloying. The addition of Y_2O_3 nanoparticles increases the mechanical properties at elevated temperature and enhances irradiation resistance. Helium ion implantation was applied to simulate irradiation effects on these materials. The irradiation was performed using a 500 kV He ion implanter at fluences around 5×10^{15} cm^{-2} for a series of samples both at room temperature and at 600 °C. The microstructure and mechanical properties of the pristine and irradiated W-Ti-ODS alloy are compared with respect to the titanium and Y_2O_3 content. Radiation damage is studied by positron annihilation spectroscopy analyzing the lifetime and the Doppler broadening. Three types of helium-vacancy defects were detected after helium irradiation in the W-Ti-ODS alloy: small defects with high helium-to-vacancy ratio (low S parameter) for room temperature irradiation, larger open volume defects with low helium-to-vacancy ratio (high S parameter) at the surface and He-vacancy complexes pinned at nanoparticles deeper in the material for implantation at 600 °C. Defect induced hardness was studied by nanoindentation. A drastic hardness increase is observed after He ion irradiation both for room temperature and elevated irradiation temperature of 600 °C. The Ti alloyed tungsten-ODS is more affected by the hardness increase after irradiation compared to the pure W-ODS alloy.

1. Introduction

Tungsten and tungsten alloys are currently considered promising candidates for plasma facing components in future fusion reactors, in particular for the divertor and first wall components [1]. As a high-Z material, tungsten has a low sputtering erosion rate, a high thermal conductivity, high mechanical strength and a high melting temperature. Drawbacks of the material are its brittleness with a ductile-brittle transition temperature around 400 °C, a significant grain growth at elevated temperature and a low recrystallization temperature. Two possible strategies are considered to increase W ductility: alloying and nanostructuring [2–5]. W materials are usually fabricated by powder metallurgy due to their high melting point. When processing W alloys, mechanical milling is a critical step for alloying and attaining both grain refinement, homogeneous solution and dispersion of nanosized particles. Addition of Ti acts as a sintering activator and increases the degree

* Corresponding author.
E-mail address: asta.richter@th-wildau.de (A. Richter).

http://dx.doi.org/10.1016/j.jnucmat.2017.07.039
0022-3115/

of densification. Titanium has limited solubility in W, so that only small contents of Ti up to 10 wt% are reported in the literature [2–5] and the melting temperature remains close to that of pure tungsten. Ti addition also alters the core structure of screw dislocations and their slip mechanism and thus increases the W ductility [1]. Y_2O_3 nanoparticles inhibit grain growth, strengthen the matrix and enhance oxidation resistance [2]. A detailed study is given by Chen et al. [5–7]. Furthermore, nano-grained and dispersion strengthened materials should be more radiation resistant than pure W and standard grain-sized materials, as the numerous grain boundaries and interfaces between matrix and particles act as sinks for the irradiation-induced defects.

In nuclear reactors, the materials structure suffers from the intensive irradiation environment. In fission, the major irradiation effect comes from neutrons and α particle irradiation. Neutron irradiation will cause a continuous production of He by nuclear reactions. In fusion He is also produced by the fusion reaction. The combined presence of gas and defects causes microstructural and morphological modifications in the material and changes the mechanical properties, which might negatively affect the performance of the tungsten alloy. The need for fundamental insight into the mechanisms that drive the microstructural evolution has motivated a wide range of experimental studies [8–11].

A simulation of the irradiation damage induced by energetic particles in the reactors can be achieved by applying ion beam irradiation at room temperature and elevated temperatures [10–13]. Helium ion implantation at a relatively low flux and low fluence in tungsten was used to investigate the early stage of helium irradiation [8]. The existence of helium in tungsten results in the formation of open volume defects such as vacancies, vacancy clusters, voids, and bubbles. At room temperature (RT), the migration energy of He interstitials in tungsten is very low. He atoms are highly mobile in defect-free tungsten and they tend to aggregate and to be trapped by the open volume defects and He-vacancy complexes He_nV_m are generated. There is also a “self-trapping” effect for the He atoms in tungsten. Due to their large binding energy the implanted He can form interstitial He-He clusters in tungsten. This effect results in the surface accumulation of He in implanted tungsten. When the number of He atoms in the clusters is increased, the surrounding tungsten atoms can be displaced from their lattice sites and He_nV_m defects are again created. The open volume defects, especially the helium-filled bubbles, play a significant role in a deterioration of the mechanical properties of tungsten and result in the surface swelling and embrittlement of the material [8–11,14]. Theoretical investigations [15–18] study intensively the mobility of these He-vacancy complexes in tungsten and model self-trapping of He and trap mutation. In particular, the migration properties of the He_nV_m defects and their interaction with point defects created by irradiation and other defects in the material are of fundamental as well as practical interest.

Tungsten-titanium alloys doped with Y_2O_3 are new, potentially high performance materials that might have improved mechanical properties compared to pure tungsten under extreme irradiation conditions. This paper therefore investigates the process of defect formation in these ODS alloys after implantation by He ions at room temperature and at 600 °C. Defect formation in the non-irradiated and irradiated W-Ti-ODS alloys is studied by positron annihilation spectroscopy which enables an analysis of the He-vacancy complexes. The resulting changes in hardness are investigated by nanoindentation. Vacancy-type defects created by helium implantation in the W-Ti-ODS alloys and their impact on nanohardness characteristics are correlated with the investigations of microstructural changes analyzed by positron annihilation.

2. Experimental

2.1. Sample preparation

Pure tungsten and titanium powders used as starting materials for mechanical alloying have an average particle size of 2–6 μm (purity >99.95%) and 48 μm (purity >99.9%), respectively. Reinforcement was obtained by addition of yttrium oxide (Y_2O_3) powder of 99.99% purity with a particle size in the range 20–50 nm. The material used in the present study is of composition W-x%Ti-y% Y_2O_3 (wt.%) with x = 0, 1 or 2 and y = 0.5 or 2.0. Hereafter the four model alloys will be referred to as W 0.5%Y_2O_3 (W-ODS), W 1%Ti 0.5Y_2O_3 (W-1Ti-ODS), W 2%Ti 0.5Y_2O_3 (W-2Ti-ODS) and W 2%Ti 2% Y_2O_3 (W-2Ti-2ODS). The elemental powders of tungsten and titanium with yttrium oxide nanoparticles were milled for 24 h using a planetary ball mill (Retsch PM 100) with a speed of 350 rpm under an argon atmosphere. Milling experiments were performed by using a tungsten carbide grinding medium with a ball to powder ratio of 10:1. The process control agent stearic acid was used to inhibit agglomeration of powders during ball milling. The mechanically alloyed powders were consolidated into green compacts with a pressure of 350 MPa and were further sintered in a mixed hydrogen-argon atmosphere at 1500 °C for 30 min. Phase characterization of the synthesized powders was conducted using X'PERT PRO X-ray diffraction (XRD) with Cu Kα radiation. The microstructure of the milled powders and sintered specimens was examined using a Hitachi-4700 SEM (see details in Chen et al. [5–7]).

The microstructure of the alloys consists of tungsten grains surrounded by a Ti(W) solid solution. The tungsten ductility is increased by Ti alloying as an effective binder phase resulting in a homogeneous microstructure and a reduced porosity. The Y_2O_3 nanoparticles stabilize the beneficial microstructure. However, high-energy ball milling can facilitate a solid-state reaction between Y_2O_3 particles and the tungsten-titanium matrix during the sintering process, which promotes the formation of stable complex nanoscale Ti-Y-O oxide particles leading to a significant increase in hardness and elastic modulus [5–7].

2.2. Ion implantation

He ion irradiation was performed using the 500 kV ion implanter (High Voltage Engineering Europe B.V., model B8385) at the Ion Beam Center (IBC) at Helmholtz-Center Dresden-Rossendorf. The He ion beam was generated using an IHC Bernas-type ion source with He gas feed, subsequently mass-separated, accelerated and electrostatically raster scanned (fx,y ~1 kHz) over the samples in the irradiation chamber. The ion beam current was measured using 4 F cups (with secondary electron suppression) situated around the samples. An ion beam current density of 1.35 μA/cm^2, corresponding to an ion flux of ~2 × 10^{12} cm^{-2} s^{-1}, was used. Samples were clamped with W needles on a heatable sample holder. The temperature was recorded using a resistance thermometer. The heating stage was tilted 7° with respect to the ion beam. A vacuum smaller than 2 × 10^{-6} mbar was maintained in the irradiation chamber.

Tungsten lattice atoms are displaced by the He implantation with ion energy between 290 keV and 350 keV and Frenkel pairs, vacancies and interstitials are created. A total number of 130 vacancies per implanted He ion was calculated by TRIM 98 [10]. The total amount of implantation-induced vacancies increases with increasing He fluence. He irradiation was performed with a cumulative set of four subsequent He ion beams of different energy and fluences as indicated in Fig. 1. Ion energies of 350, 320, 300 and 290 keV with corresponding fluences of 5 × 10^{15}, 5 × 10^{14}, 1 × 10^{15} and 3.5 × 10^{15} cm^{-2}, respectively, were used to adapt an

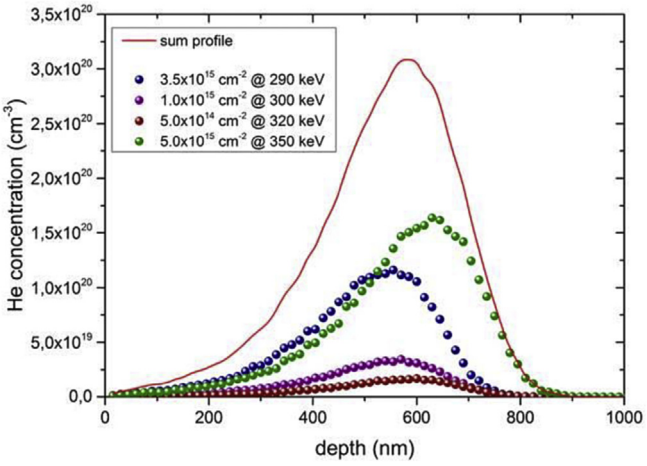

Fig. 1. He irradiation with a cumulative set of four subsequent He ion beams of different energy and fluence resulting in the sum profile with a maximum of He concentration at 580 nm depth (calculation with 2008 SRIM [19] code for pure tungsten).

implantation profile applied in former investigations for comparison with pure tungsten material [10]. The He implantation profile (Fig. 1) was calculated with the 2008 SRIM code for pure tungsten [19] and shows a maximum He concentration at 580 nm depth. The depth profiles of the implantation-induced vacancies are shifted slightly towards the surface compared to those of the implanted He ions. The formation of helium-vacancy (He_nV_m) clusters is correlated with a variation of the local ratio of He atoms and implantation-generated vacancies as calculated in Refs. [9,10]. Since He diffuses in tungsten much faster than the radiation induced W interstitials, the large number of induced vacancies will act as traps for the implanted He.

Two sets of samples with equal chemical composition have undergone an irradiation with a cumulative set of four subsequent He ion beams of different energies and fluence as described above. One set of samples was irradiated at room temperature (RT) without additional heating. The temperature of these samples increased only from 30 to 70 °C during ion irradiation due to ion beam induced heating. The other set of samples was He implanted under the same parameters, but with additional heating at a fixed temperature of (600 ± 10) °C.

2.3. Positron annihilation spectroscopy

Positron annihilation spectroscopy (PAS) is known to be a non-destructive, powerful technique to detect sub-nm sized open volume defects in metals. Two positron-annihilation techniques are employed at HZDR. Positron-annihilation lifetime-spectroscopy (PAS-LT) measures the elapsed time between the implantation of the positron into the material and the emission of annihilation radiation. Doppler-broadening spectroscopy (DBS) employs the energy-momentum conservation during positron annihilation. Using mono-energetic positron beams, depth-dependent defect characterization of thin films can be performed.

2.3.1. Positron lifetime measurements

In order to characterize the pristine state of the W-Ti-ODS samples PAS-LT was applied. The LT measurements were carried out using a conventional lifetime system. The sample was arranged as a sandwich made from two identical sample pieces with a ^{22}Na source as positron emitter in between. Calibration of the time resolution of the apparatus was first performed with Si samples having a single positron lifetime component of 218 ps? The result was 220.9 ps? The contribution of the Al sealed positron source to the spectra was corrected according to the procedure given in Ref. [20].

2.3.2. Doppler broadening spectroscopy

In order to identify the nature of the defects created by He implantation, positron annihilation Doppler broadening spectroscopy (DBS) was applied. DBS is an excellent technique to detect open volume defects from clusters consisting of several vacancies down to less than a mono-vacancy. The positron in a crystal lattice is strongly subjected to repulsion from the positive atom core. Because of the locally reduced atomic density inside the open volume defects with a lower local electron density, positrons have a high probability to be trapped and to annihilate with electrons in these defects by the emission of two 511 keV photons. DBS monitors the annihilation radiation of the 511 keV photons. The Doppler broadening of the 511 keV annihilation line is mainly caused by the momentum of the electron due to the very low momentum of the thermalized positron. There are two main parameters, S (shape) and W (wing), obtained from the 511 keV annihilation line. The S parameter reflects the fraction of positrons, annihilating with electrons of low momentum (valance electrons). Therefore, the S parameter is mainly a measure for the open volume in the material. It is defined as the ratio of the counts from the central part of the annihilation peak (here 510.03 keV–511.17 keV) to the total number of counts in the whole peak (here 498 keV–524 keV). The W parameter is defined as the ratio of counts in the two wings of the annihilation spectrum (513.16–514.13 keV and 507.87–508.84 keV) to the total number of counts in the peak. The W parameter corresponds with the annihilation of the high momentum electrons (core electrons) and describes the chemical surrounding of the open volume.

DBS measurements were carried out with the mono-energetic slow positron beam “SPONSOR” at HZDR [21,22] at which a variation of the positron energy E from 30 eV to 36 keV with a smallest step width of 50 eV, if required, is possible. The energy resolution of the Ge detector at 511 keV was (1.09 ± 0.01) keV, resulting in a high sensitivity to changes in material properties from surface to a depth of several μm.

2.4. Nanoindentation

The mechanical properties of W-Ti-ODS samples were investigated by nanoindentation (NI) [23,24]. NI is a suitable method to determine the mechanical properties of a thin irradiated surface layer, since depth dependent mechanical quantities such as hardness and indentation modulus are obtained. NI measurements were performed at room temperature using the electrostatic transducer of the UBI Hysitron triboscope with a 90° cube corner tip. Depth dependent mechanical properties were obtained by multi-cycling indents [25] with repeated loading and unloading at the same location on the sample surface. The set of data includes the entire material response, from the first indenter-to-sample contact down to the maximum penetration depth. All load–displacement curves were analyzed according to the standard Oliver–Pharr method [23]. The NI measurements were performed before and after ion implantation at room temperature.

A thin layer of hard material on top of a softer matrix material represents a complex layer system, which is very sensitive to the softer matrix unless the indenter penetrates the overlying hard layer. This complicates the hardness measurements. To avoid this effect, the indentation depth should be less than 10% of the hard layer thickness (Bückle rule [24]). It means an indentation depth less than 60 nm according to the ion range profile (see Fig. 1).

Although hardness values at very shallow penetration depths have been recorded, indentation measurements have been performed up to a depth of 200 nm with an applied maximum load of 7 mN or less. Thus, the hardness depth profile is smeared out and the indentation depth scale does not necessarily represent the real depth profile. Additionally, a strong increase of the hardness for small penetration depth is observed in lots of materials, especially in metals which is known as the indentation size effect [26]. These problems, to be considered by measuring the hardness of a narrow implanted layer, are well addressed by Hosemann [27].

3. Results and discussion

3.1. Non-irradiated W-Ti-ODS alloys

3.1.1. PAS results

Positron lifetimes were calculated for the non-irradiated W-Ti-ODS samples with the PALSfit program package [22,28] and are displayed for the different materials in Table 1. All samples clearly show two different life times in the range of τ_1 ~115 … 124 ps and τ_2 ~ 249 … 327 ps? The positron lifetime in a defect-free single crystal of tungsten is τ(W) ~ 105 ps and the estimated positron lifetime in mono and di-vacancies in tungsten is reported to be τ_{v1}~136 ps and τ_{v2} ~157 ps, respectively [11,29]. Nano-voids having 13–37 vacancies in tungsten have a theoretically calculated positron lifetime of 410 … 440 ps [30]. However, the experimental identification of defects characterized by lifetimes of more than 300 ps is not straightforward.

Since all samples contain Y_2O_3 nano-particles, special attention is given to the positron lifetime of defects in that component. Defects with a lifetime of 212 ps were observed in Y-containing ODS alloys [31]. These defects are not yet completely identified, but are surely related to positron annihilation at the interface of Y–Al oxide nanoparticles. Similar defects with a lifetime of 288 ps … 275 ps corresponding to 4–5 vacancies in connection with yttrium oxide were reported by Koegler [12,32].

The observed positron life times in the non-irradiated W-Ti-ODS materials (Table 1) are attributed to pre-existing defects of different sizes generated by the sample manufacturing process. The W 0.5% Y_2O_3 material has a high amount of 85% of the short positron lifetime defects characterized by τ_1 reflecting defect states corresponding to mono- and di-vacancies. The 15% with positron lifetime $\tau_2 = 300$ ps indicates nano-voids. The second lifetime of τ_2 could be also related to nano-voids correlated with Y_2O_3 nanoparticles.

The addition of titanium in W-Ti-ODS increases the positron lifetime τ_1 slightly, however, the intensity of this component increases drastically to 96% and 92% for addition of 1% and 2% titanium, respectively. The lifetime of positrons trapped in mono-vacancies in titanium is reported to be 220–240 ps and the positron lifetime in titanium oxide is 190–200 ps [33]. Both lifetimes could not be verified in the lifetime spectra of the pristine samples. The second component lifetime τ_2 is again characteristic for vacancy clusters and does not change too much in the W 1–2%Ti 0.5% Y_2O_3 compared to the W 0.5%Y_2O_3 sample, however the intensity is strongly reduced. It is not so easy to distinguish between all these contributions to identify different defects in a proper way, however, it is obvious, that the size and number of larger nano-voids is reduced in the W-Ti-ODS alloys with 1–2% Ti compared to the W-ODS. It is also confirmed by electron microscopy investigations that a homogeneous microstructure with a uniform distribution of Ti-rich oxide particles was fabricated by the addition of titanium [5].

An increase of Y_2O_3 nanoparticles in the W-Ti-ODS alloy to 2% (W 2%Ti 2%Y_2O_3) changes the positron lifetimes and their intensities again. τ_1 ~ 115 ps is lower than the lifetimes of the other W-Ti-ODS alloys and with an intensity of 87% comparable to the vacancy-type defects in W-ODS. A low annihilation probability with high momentum electrons is observed for Y_2O_3 with a high positron affinity [12,34]. These properties influence the second positron lifetime τ_2 ~ 249 ps, which is dramatically smaller than the life times in all other W-Ti-ODS alloys. This indicates that vacancy clusters are correlated with Y_2O_3 nanoparticles and that the nano-voids are definitely smaller. Thus, the higher amount of 2% Y_2O_3 decreases both positron lifetimes indicating smaller defects due to the Y_2O_3 nano-dispersoids.

Table 1 gives a summary and also displays the weighted average positron lifetimes, which are smaller for all alloys containing titanium compared to the W-ODS. That means, the concentration of vacancy clusters is less in the W-Ti-ODS alloys compared to the W-ODS.

Fig. 2 shows the S parameter versus the positron energy E of the non-implanted samples. A comparison of S(E) of the W-Ti-ODS with pure and well-annealed W is given in order to show the influence of the Ti and Y_2O_3 additives on this parameter. The higher S value of W-ODS and the W-Ti-ODS is attributed to pre-existing vacancy-type defects, which were generated by sample manufacturing. The S parameter starts with high values at low positron energies, which is caused by the positron annihilation at the surface. The S parameter of the W-ODS sample without Ti decreases to a minimum at an energy of 0.5 keV, which is a sign of a small oxide layer of only a few nm at the surface. The peak at 3 keV represents the influence of sample polishing and the consequent generation of defects beneath the surface. The titanium containing W-Ti-ODS alloys have a bigger hardness implying that defect generation by polishing is reduced and so not visible in such a pronounced peak in S. The S parameter of the highest positron energy represents the value of the bulk samples. It is seen that S_{bulk} is

Table 1
Results of the positron lifetime spectroscopy for W-Ti-ODS alloys as specified with lifetime peaks and their respective intensities. The positron mean lifetime τ_{av} is the weighted average of two lifetime values.

Material	τ_1 [ps]	I_1 [%]	τ_2 [ps]	I_2 [%]	τ_{av}[ps]
W 0.5%Y_2O_3	119	85	300	15	147
W 1%Ti 0.5%Y_2O_3	124	96	327	4	133
W 2%Ti 0.5%Y_2O_3	122	92	286	8	135
W 2%Ti 2%Y_2O_3	115	87	249	13	133

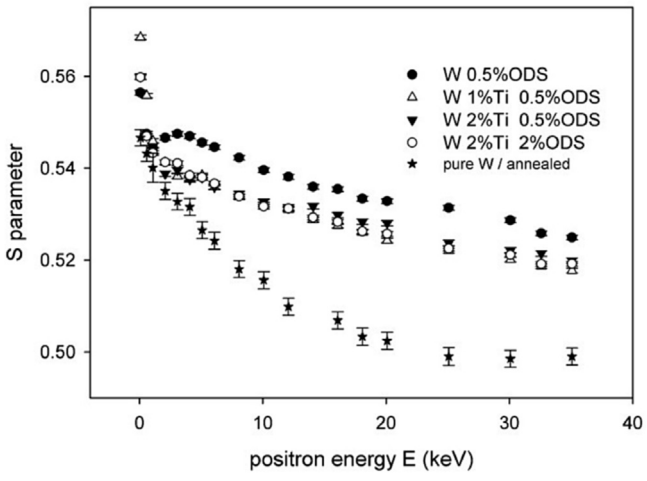

Fig. 2. S parameter versus positron energy of the virgin W-Ti-ODS samples as indicated compared to well-annealed pure tungsten.

reduced with Ti additives. That implies that the addition of up to 2% titanium results in a better densification of the W-Ti-ODS alloys with a fine grain structure [5].

3.1.2. Nanoindentation results

Nanoindentation hardness measurements do not reflect all the details visible in the positron lifetime measurements. In the non-irradiated samples, the pre-existing manufacturing defects such as impurity clusters, grain boundaries, and dislocation loops make a significant contribution to the hardness. They can serve as pinning sites against the movement of the dislocations. The reduction of the density of such defects by thermal treatment weakens the pinning effect and reduces significantly the hardness [12,35].

The hardness data represent an average value determined from a minimum of 10 separate indentation values. In general, the error in the hardness values is below 5% and is not explicitly marked in the figures. There is a drastic hardness increase for the alloying with titanium compared to the W-ODS sample (Fig. 3). Since the indentation hardness of all titanium containing alloys is within the standard deviation of less than 5%, only a typical depth dependent hardness curve is presented in Fig. 3. The hardness increase is about 2.5 GPa or about 45% compared to the hardness of 5.3 GPa in W-ODS. The increase in hardness in the titanium containing W-Ti-ODS alloys has been ascribed to a homogeneous and dense microstructure with the formation of TiO_2 and fine $Ti_2Y_2O_7$ oxide particles uniformly dispersed in the matrix [5]. The dispersed oxide particles act as pinning points to obstruct grain growth and dislocation movement. It is assumed that strengthening by the oxide dispersoids in the W-Ti-ODS alloys is critically dependent on the strength of the bond between oxide particles and the matrix. In the case where titanium strongly interacts with Y_2O_3 during ball milling and subsequent sintering, the formation of uniformly combined Ti-rich Ti-Y oxide particles was promoted. Hence, the interfacial bond between the oxide particles and the matrix is stronger in the W-Ti-ODS alloys. Local hardness variations close to the sample surface have been observed in the titanium containing W-Ti-ODS samples. However, a well pronounced hardness maximum was not visible in the non-irradiated samples.

3.2. He implanted W-Ti-ODS alloys

3.2.1. PAS results

The existence of helium in W-Ti-ODS alloys results in the formation of open volume defects where He atoms are trapped, forming He-vacancy complexes in the form of He_nV_m [9,10]. According to theoretical model calculations [15,16,18] these He_nV_m defects are formed by vacancy generation during bombardment

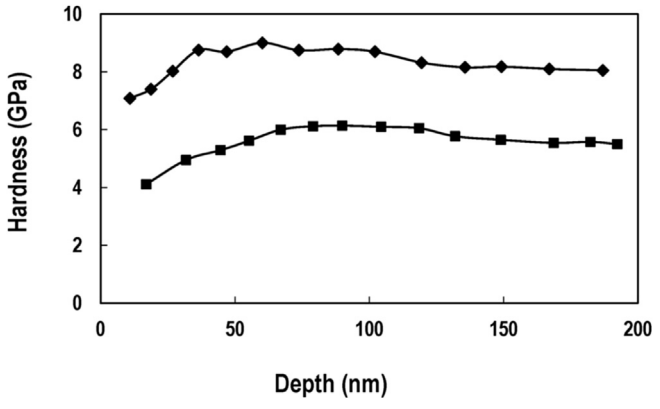

Fig. 3. Depth dependent indentation hardness profiles of non-irradiated W 0.5%Y_2O_3 (■) and W 2%Ti 2%Y_2O_3 (◆).

where the He ions are pinned. He content inside the vacancies prevents the annihilation with the low momentum electrons of tungsten and promotes the positron annihilation with He electrons having higher momenta. As a consequence, the Doppler broadening of the annihilation line increases and the S parameter decreases, compared to annihilation in free open volume.

Another process is the “self-trapping” effect for the He atoms in tungsten that results in He interstitial clusters. Due to their large binding energy of the order of 1 eV, the implanted He can form interstitial He-He clusters. This effect also results in the accumulation of He and has been reported in implanted tungsten [16,17]. When the number of He atoms in the clusters increases, the surrounding metal atoms can be displaced from their lattice sites and He_nV_m defects are created. Because these defects are formed through the trap mutation process without the benefit of existing vacancies the He to vacancy ratio is expected to be higher than that found when He diffuses and is trapped by existing vacancy clusters. Although the He concentration in these defects is very high, they still serve in PAS as efficient traps for positrons and result in an increased S parameter [9]. A trap mutation process is not expected during He implantation in our sample series and implantation conditions.

The He-to-vacancy ratio is a very sensitive factor that controls the S-parameter in positron annihilation experiments. An increase of the S parameter could be caused either by an increase of the size of He-V clusters or by the increase of their density. However, reduction of the He-to-vacancy ratio due to e.g. coalescence or Ostwald ripening reduces also the S parameter. Therefore, the S-parameter cannot distinguish between different growth processes of the He filled vacancies. The formation process of nanovoids is not yet fully understood in these materials. However, differences in the defect formation in He irradiated Y_2O_3 doped W-Ti alloys are noticed in comparison to defect formation in pure tungsten. The S parameter profiles dependent on positron energy are shown in Fig. 4 for W-Ti-ODS alloys before and after He implantation. The S parameter is clearly increased for all model alloys for both He implantation at room temperature and at 600 °C. An increasing S parameter corresponds to a larger size and a higher concentration of open volume defects, but reflects also the helium filling in the nano-voids. For 600 °C temperature implantation, two pronounced maxima are visible, one very close to the surface at 2 keV and a second broad one at about 18 keV. These features are less pronounced in the S profiles for implantation at room temperature and for the high temperature implanted W 2Ti 2 ODS sample.

The S(E) plot implicitly contains the depth distribution of open volume defects. For instance, a numerical solution of the positron diffusion equation with the assumption of a Makhovian implantation profile for the positrons can be applied in order to fit S(E) to a depth dependent S parameter profile. The software package VEPFIT is a fast method for such a numerical solution. The procedure was described in detail by Ou et al. [10]. Application of the method shows, that the second broad maximum in the S-E plot in the W-Ti-ODS alloys corresponds to the maximum of the He concentration in the SRIM implantation profile around 580 nm. The first maximum of the S-parameter for high temperature implantation is close to the surface at about 30 nm. Such a peak was not observed in the irradiated pure tungsten [10]. The position of this peak is unlikely to be correlated with the maximum defect and He concentration in the damaged layer, but is attributed to more defects close to the surface due to sample manufacturing and high mobility of vacancies and He ions. An implanted He driven microstructure evolution close to the surface is also discussed in model calculations for tungsten in Ref. [17].

The broad plateau in the S-E plot for HT and also RT implantation corresponds to the maximum of the He concentration in the SRIM

implantation profile. Broader peaks in the S parameter indicate a deeper defect distribution. Implanted He atoms are trapped by the open volume defects at the Y-Ti oxide nanoparticles' interface with the alloy and are homogeneously distributed over the the implanted layer (Fig. 4). Such He-vacancy clusters might be more stable than the empty vacancy clusters due to He accumulation inside the open volume. The S parameter in Fig. 4 reflects the simulated damage profile created by He ion irradiation (Fig. 1). Beyond the maximum values, the S parameter decreases gradually when the mean incident depth increases due to the decline of irradiation induced damage and He concentration. Thermal migration of the interstitial He to surface might affect the slopes of the S-E plots.

The S parameter of W-Ti-ODS alloys at room temperature is larger than for the non-irradiated materials, but lower than that for 600 °C temperature implantation. In RT irradiated samples, the mobile He atoms are redistributed and preferentially trapped by the ion generated vacancies in the region with low He-to-vacancy ratio or by the pre-existing surface defects in the same region. At an irradiation temperature of 600 °C, the small He_nV_m, m = 0,1,2 are more mobile and may form larger complexes preferentially closer to the surface. The influence of heat treatment during He implantation or after irradiation was investigated in detail for pure tungsten [9,10] by PAS measurements and a similar behavior for the S-parameter was reported as found in the W-Ti-ODS alloys. However, in the W-Ti-ODS these vacancy complexes may also be pinned at the surfaces of the Ti-Y-O oxide nanoparticles.

The thermal stability of helium–vacancy clusters in W-Ti-ODS alloys might be indicated by the observed dominant surface peak in the S(E) plot for 600 °C implantation. This peak has almost disappeared in the S parameter profiles for RT irradiation and also for the W 2%Ti 2% Y_2O_3 with increased Ti-Y-O nanoparticles both at RT and HT irradiation (Fig. 4c). It is likely that He-vacancy complexes diffuse towards the surface at high temperature and coalesce there. Theoretical model calculations [16,17] show, that the stability of such objects is a competitive process depending not only on temperature but also on the helium-to-vacancy ratio in mixed clusters or helium number in pure interstitial helium clusters. If the Ti-Y-O nanoparticle concentration is increased as in the case of the W 2%Ti 2% Y_2O_3 sample, the He_nV_m complexes are smaller and may be associated with He trapping at the nanoparticle interface, so that the formation of self-trapping He-vacancy complexes in combination with interstitial He clusters is suppressed. This is reflected in the plateau-like S-parameter profile for RT and HT implantation for 2% Y_2O_3 concentration and differs a lot from the dominant two peak plot for W-Ti-ODS alloys with lower Y_2O_3 concentration.

In Fig. 5 the S-W plot of the investigated materials is displayed, which allows a direct comparison of defect types in the different samples. All the data points, which lie on a straight line in the S-W plot represent the same type of open volume defects. The slopes of the straight lines, however, are different and imply the formation of different kind of defects in the RT and HT implanted W-Ti-ODS alloys.

A comparison of the defect types can be distinguished by the lines in the S-W plot with former investigations on pure tungsten without additional alloying elements and ODS particles and is given in Fig. 5a.

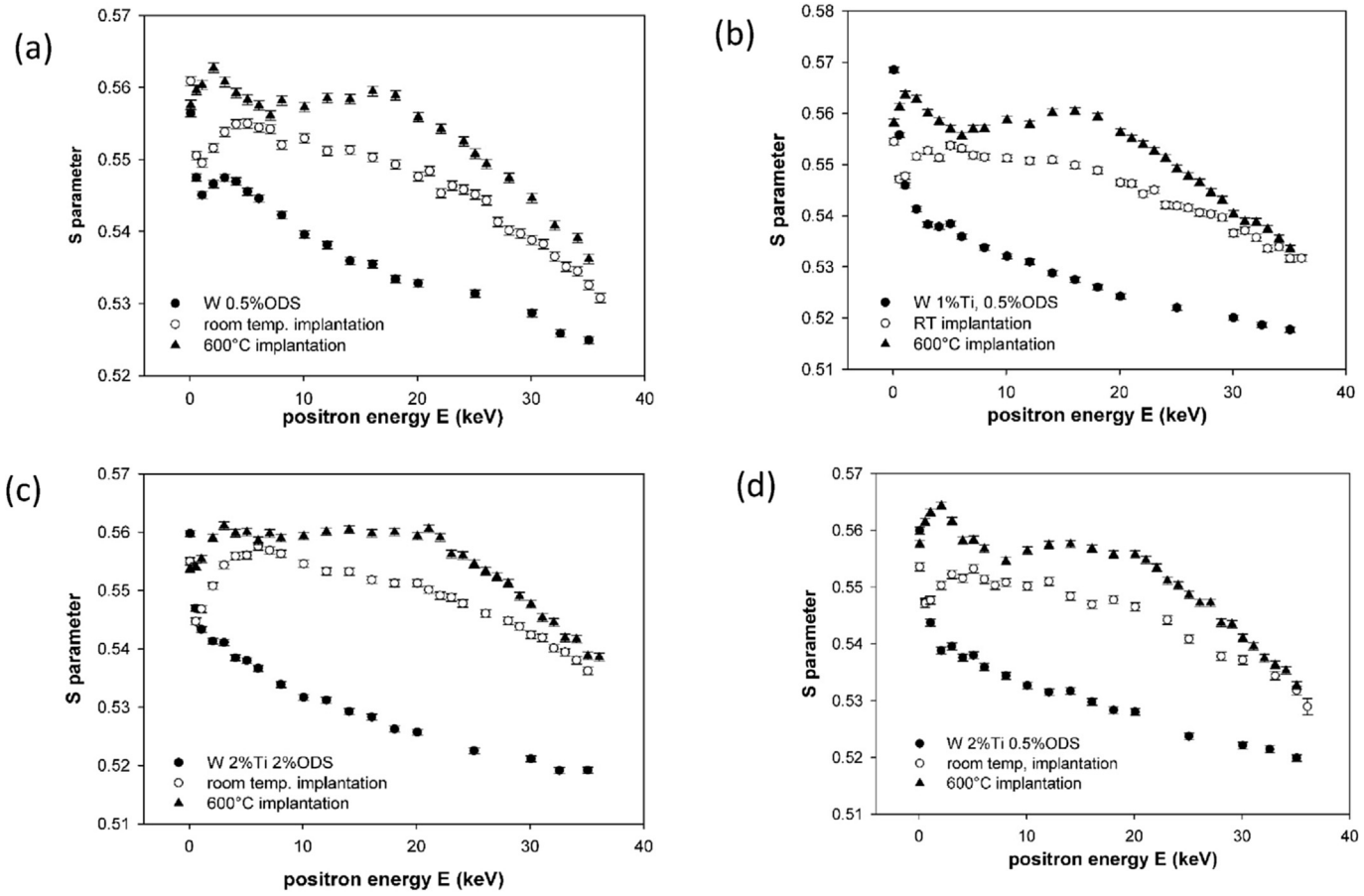

Fig. 4. S parameter versus positron energy of several W-Ti-ODS samples in comparison of non-irradiated, RT He implanted and 600 °C He implanted samples: (a) W 0.5%Y_2O_3, (b) W 1%Ti 0.5%Y_2O_3, (c) W 2%Ti 2%Y_2O_3, (d) W 2% 0.5%Y_2O_3.

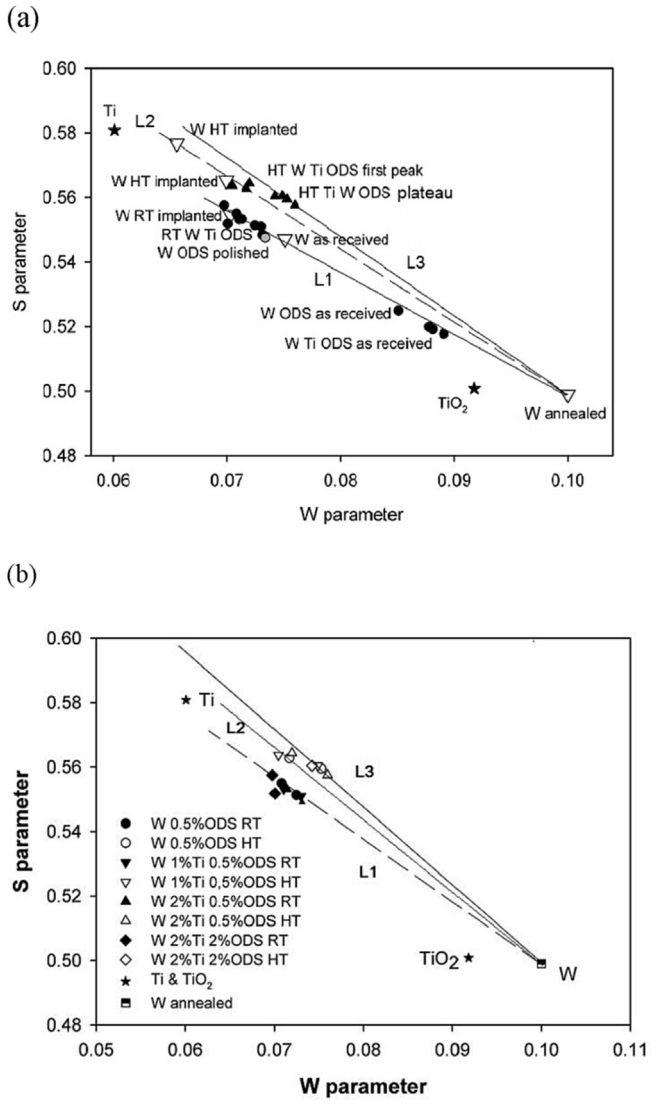

Fig. 5. S-W plot of virgin and He implanted W-Ti-ODS alloys: (a) comparison with pure tungsten (∇) [10] and (b) details for W-Ti-ODS alloy as indicated. W1 and W2 refer to fluences of 5×10^{15} cm^{-2} and 1×0^{16} cm^{-2}, respectively, in pure tungsten. Lines L1, L2 and L3 mark different defects.

Pure tungsten and non-irradiated materials exhibit a low S and relatively high W parameter. Data points are positioned along line L1 and represent the same type of defect. The defect formation by He implantation at RT results in very similar defects for pure tungsten, W-ODS and W-Ti-ODS samples. It is clearly visible that the non-irradiated ODS samples are characterized by a smaller open volume compared to the pure W as received [10].

In fact, the trend indicated by the lifetime measurements (Table 1) is also reflected in the S-W plot where the open volume of W-ODS is slightly larger than that of the titanium containing W-Ti-ODS alloy. The peak in the near surface region of non-irradiated W-ODS (W ODS polished) has a comparable number of open volume defects as the virgin W (W as-received) investigated in Ref. [10]. This peak is attributed to pre-existing vacancy-type defects in the surface region of the W-ODS sample, mainly dislocation loops and impurity clusters which were generated by the sample manufacturing and surface polishing.

The S and W values for titanium and TiO_2 are measured and also displayed in Fig. 5a. The effect of Ti as an alloying material or TiO_2 cannot be resolved in the S-W plot. The type of defect formation is not changed by the titanium content nor the formation of TiO_2. Only the size of the vacancy clusters and after He irradiation the type of the He-vacancy clusters is modified, which seems to be caused by the addition of Y_2O_3 nanoparticles.

Details for the W-Ti-ODS alloy for RT and HT implantation are presented in Fig. 5b. Three types of defects can be distinguished on each line marked with L1, L2 and L3. For RT implantation, the defects identified close to the surface and deeper in the implanted area are of the same type (line L1). However, the vacancies at the surface are slightly bigger compared to the He-vacancy clusters located at larger implantation depth (see also Fig. 4).

The near surface peaks of the S parameter in HT irradiated W-Ti-0.5% ODS alloys (Fig. 4) appear as separate points in the S-W diagram along line L2. Thus, the formation of near surface defects corresponds to another defect type. These defects reflect the largest open volume detected by PAS in the W-Ti-ODS alloys. This surface peak is suppressed in case of W 2%Ti 2%ODS and a related data point is missing on line L2. As seen in Fig. 4c, the distribution of the open-volume defects is much broader and the S parameter is higher for this sample than for the samples with only 0.5% ODS. That suggests that the homogeneously distributed ODS pins the He-vacancy complexes around the interface.

HT implantation in all W-Ti-ODS alloys is typically presented by the broad plateau of the S parameter. The corresponding S-W data are all along line L3. These He-vacancy defects on line L3 represent the influence of the Ti-Y-O oxide nanoparticles, which reduces the growth of He-vacancy complexes elsewhere. We call these defects He_nV_m-ODS defects.

Basically, all the observed open volume defects in He irradiated W-Ti-ODS are He-vacancy defects. The difference between the L1, L2 and L3 defects can be related to the different size and the very different He-to-vacancy ratios. He-vacancy complexes at RT implantation result in a high He concentration in the He-vacancy clusters. The vacancy clusters homogeneously nucleate under irradiation in the matrix of grains and the yttrium oxide particles attract and accumulate vacancies, but prevent formation of large He-vacancy complexes. For comparison, the S-W data for pure tungsten implanted at room temperature under the same conditions are displayed in Fig. 5a. The S-W data points of non-irradiated and at RT implanted pure tungsten and W-Ti-ODS alloys are all positioned on line L1 and represent the same type of defect. The higher S parameter for implanted material represents He-vacancy complexes with high He-to-vacancy ratio.

The S parameter increases for 600 °C He implantation both for pure tungsten and W-Ti-ODS.

The increased mobility of He-vacancies at elevated temperature supports growth of complexes with a low He-to-vacancy ratio. It is interesting that the He-vacancy defects generated in pure tungsten [10] for HT implantation of fluence 5×10^{15} cm^{-2} and 1×0^{16} cm^{-2} are found on line L2 in the S-W plot in Fig. 5a. These defects represent a large open volume close to the surface and also at larger implantation depth for pure tungsten. For the W Ti 0.5%ODS alloys the defects represented on line L2 are He-vacancy complexes close to the surface. The main response of the W-Ti-ODS alloys to the He HT implantation is indicated by the defects represented by line L3. This means the effect of the ODS particles is reflected by the S-W data points on line L3. It is clearly seen, that the open volume of the ODS samples is diminished and the He-vacancy complexes are smaller compared to that in pure tungsten. At resulting fluences of 1×10^{16} cm^{-2} for HT He implantation in W-Ti-ODS, the defect concentration is explicitly lower than the open volume generated in pure tungsten under the same conditions. The reason is the formation of a homogeneous distribution of small He-vacancy complexes He_nV_m with low He concentration over the whole implantation range, when nanodispersed oxide particles pin the

vacancies. The effect of the ODS particles is less for room temperature implantation, but results in another type of He-vacancy with larger He-to-vacancy ratio for HT implantation. The higher ODS concentration reduces the He diffusion to the surface.

3.2.2. Nanoindentation results

The hardness of the implanted W-Ti-ODS alloys strongly depends on the type, size and density of the defects created in the damaged layer by implantation. The hardness values of all implanted samples are higher than the value of the non-implanted sample, which means that implantation hardening occurs for all irradiation temperatures in W-Ti-ODS alloys. Dislocation loops, vacancy-like defects and small volume defects are generated in the implantation layer of the samples, which act as pinning points to impede the motion of dislocation lines and increase the hardness.

For all depth dependent hardness curves of the implanted W-Ti-ODS samples (Fig. 6), hardness maxima are observed. The penetration depths for the peak values vary with composition, but are all more shallow than the depth for the maximum He concentration displayed in Fig. 1. Keeping in mind the complex layer system of a hard implanted surface thin film on a soft bulk matrix, the application of the 10% Bückle rule correlates the hardness maximum with the damage profile of the SRIM calculations (Fig. 1). Thus, the hardness decline from the surface toward the bulk, has been explained by the generated defects during He implantation. Results for all W-Ti-ODS samples are given in Table 2 and Fig. 6.

The W 0.5% Y_2O_3 sample (Fig. 6a) shows a distinct hardness maximum of 9.4 GPa at 36 nm for RT helium implantation with reference to the non-irradiated alloy with H = 5.3 GPa. At an elevated implantation temperature at 600 °C, the hardness increase is lower than the value at RT implantation. For W-ODS alloys a broad hardness maximum of 8.4 GPa at around 55 nm is visible reflecting a homogeneous He filled vacancy-defect distribution in the irradiated area. The hardness maximum is shifted away from the surface into the implanted layer, which might be caused by a soft defect layer near the surface as already discussed for the PAS results.

The implantation induced hardness increase is especially high for the titanium alloyed W-Ti-ODS samples, both for implantation at RT and 600 °C (Fig. 6b). The variation of the titanium content has no influence on the hardness maximum nor the depth position. The maximum hardness value of about 16.6 GPa at 25 nm for RT implanted samples is more than double the hardness of the non-irradiated alloy with H = 8 GPa. The strong hardness increase in the W-Ti-ODS alloys after He irradiation at room temperature is attributed to the increased defect density of small He filled vacancy defects with a high He-to-vacancy ratio, which act as obstacles against dislocation motion. A larger concentration of Y_2O_3 nanoparticle of 2% changes the defect size and distribution caused by irradiation. The hardness maximum with H = 15.7 GPa for RT implantation in W 2%Ti 2% Y_2O_3 is shifted to 35 nm. A homogeneous defect distribution due to effective pinning of the He-vacancy complexes at ODS nanoparticles may cause this depth dependent hardness profile.

With increasing implantation temperature at 600 °C, the hardness increase for the W-Ti-ODS alloys is lower than the value at RT and a broad hardness maximum of about 13.6 GPa is visible. In all W-Ti-ODS alloys, the hardness maximum is shifted away from the surface into the implanted layer for HT irradiation reflecting a homogeneous He filled vacancy-defect distribution with a soft surface layer. Elevated temperatures have the effect that existing defects are partly annealed, so that the total defect density may be reduced and the hardness declines. The different depth profiles of the S parameter in PAS observed for RT and HT implantation are roughly reflected in the hardness profiles.

4. Summary and conclusion

The distribution and type of open volume defects in He irradiated W-Ti-ODS alloys are investigated by positron annihilation spectroscopy and their effect on the hardness of the material is studied by nanoindentation. In detail, the S parameters as a measure for the open volume and the hardness values are compared for the same samples. The results can be summarized as follows:

(1) All W-Ti-ODS alloys have a lower S parameter compared to the titanium free W-ODS, which means less and smaller open volume defects.

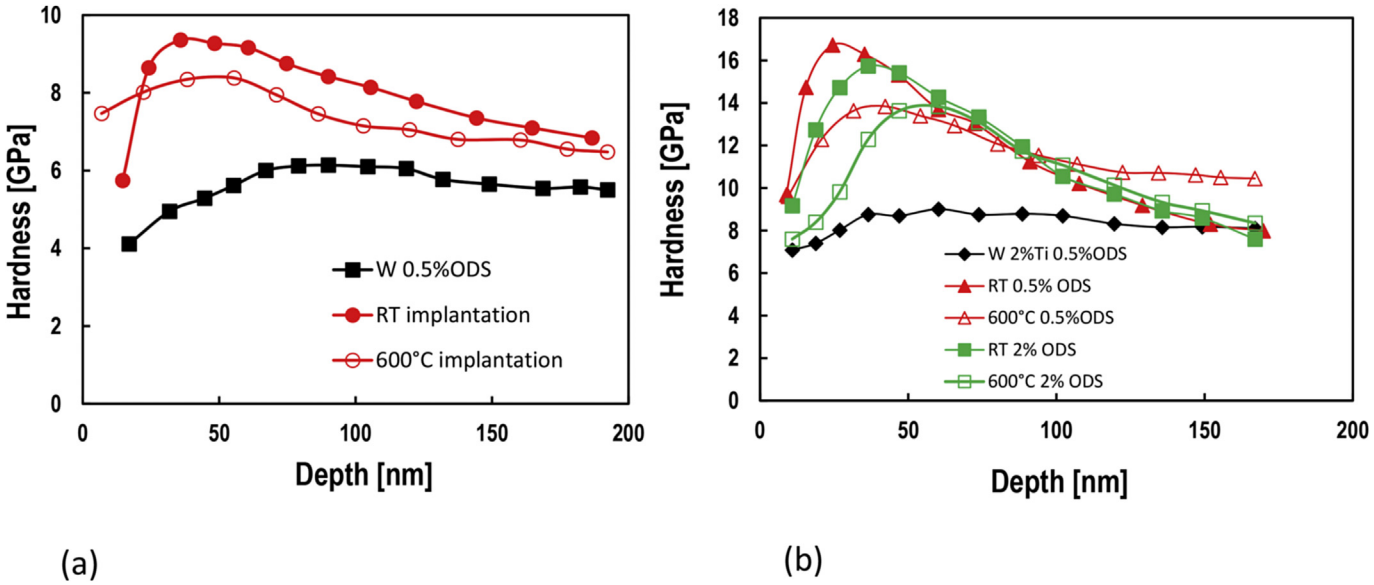

Fig. 6. Depth dependent indentation hardness profiles of non-irradiated and at room temperature (RT) and elevated temperature (HT) He implanted W-Ti-ODS samples: (a) W 0.5% Y_2O_3, (b) W 2%Ti 0.5%Y_2O_3 (▲ red) and W 2%Ti 2%Y_2O_3 (■ green).

Table 2
Indentation hardness for W-Ti-ODS alloys as specified for non-irradiated specimens. For irradiated samples, the hardness maximum with respective penetration depth for He implantation at room (RT) and elevated temperature (HT) and the hardness ratio are presented.

Material	H [GPa] Non-irradiated	H[GPa] maximum RT implantation	Depth RT [nm]	Hardness ratio H(RT)/H	H[GPa] maximum HT implantation	Depth HT [nm]	Hardness ratio H(HT)/H
W 0.5%Y_2O_3	5.3	9.4	36	1.77	8.4	56	1.58
W 1%Ti 0.5% Y_2O_3	7.8	16.5	25	2.11	13.6	41	1.74
W 2%Ti 0.5% Y_2O_3	8.0	16.7	24	2.09	13.8	42	1.73
W 2%Ti 2% Y_2O_3	8.0	15.7	35	1.97	13.4	66	1.67

(2) He irradiation of W-Ti-ODS alloys results in a higher S parameter than in the virgin material. The S parameter is even more enhanced for implantation at elevated temperature. The He-vacancy complexes in W-Ti-ODS are generally smaller than in pure tungsten due to the pinning effect of Y-Ti-O oxide nanoparticles.
(3) Three types of helium-vacancy defects were detected after helium irradiation in the W-Ti-ODS alloy: small defects with high helium-to-vacancy ratio (low S parameter) for room temperature irradiation, large defects with low helium-to-vacancy ratio (high S parameter) at the surface and the distinguished He_nV_m-ODS defects deeper in the material for implantation at 600 °C, which characterize the pinning to the nanoparticles.
(4) The hardness characteristics of implanted W-Ti-ODS alloys are clearly related to the measured S parameter profiles. It means that implantation hardening occurs which is controlled by the He-vacancy complexes.
(5) Both PAS and nanoindentation measurements could not deliver detailed conclusions about the influence of Ti on the mechanical properties in W-Ti-ODS alloys. Therefore, the presented investigation was focused on defect formation and hardness changes in He irradiated materials. Comprehensive details about the Ti influence on the mechanical properties of W-Ti alloys is given in Refs. [1,5].

Positron annihilation measurements are able to identify different types of He-vacancy defects. At RT implantation the He is immediately caught by the vacancies created during the implantation. These vacancies are pinned by the Y-Ti-O nanoparticles. Therefore, small He vacancy complexes are generated, mainly mono- and di-vacancies, which are filled with He atoms resulting in a high He-to -vacancy ratio. Similar results were obtained for RT irradiation in pure tungsten.

The situation is different for HT implantation. The broad plateau of the S parameter indicates a broad distribution of He-vacancy defects over the whole implantation layer. These defects are different from all other observed defect types and are definitely correlated with the ODS features, which are called He_nV_m-ODS vacancy complexes. These defects are different from those in pure tungsten HT implantation. In fact, the defects formed by HT implantation in pure tungsten have a larger open volume with a low He-to-vacancy ratio even for lower dose of irradiation and belong to another defect type. They have the same characteristics as the defects generated by HT implantation in W-Ti-ODS alloys close to the surface, although these complexes are smaller. The effect of the ODS pinning is less pronounced in the near surface region.

References

[1] S. Wurster, N. Baluc, M. Battabyal, T. Crosby, J. Dud, C. García-Rosales, A. Hasegawa, A. Hoffmann, A. Kimura, H. Kurishita, R.J. Kurtz, H. Li, S. Noh, J. Reiser, J. Riesch, M. Rieth, W. Setyawan, M. Walter, J.-H. You, R. Pippan, J. Nucl. Mater. 442 (2013) S181–S189.
[2] M.V. Aguirre, A. Martín, J.Y. Pastor, J. LLorca, M.A. Monge, R. Pareja, J. Nucl. Mater. 404 (2010) 203–209.
[3] B. Savoini, J. Martínez, A. Muñoz, M.A. Monge, R. Pareja, J. Nucl. Mater. 442 (2013) 5229–5232.
[4] A. Muñoz, B. Savoini, E. Tejado, M.A. Monge, J.Y. Pastor, R. Pareja, J. Nucl. Mater. 455 (2014) 306–310.
[5] C.-L. Chen, Y. Zeng, J. Nucl. Mater 469 (2016) 1–8.
[6] C.-L. Chen, Y. Zeng, Int. J. Refract. Metals Hard Mater. 56 (2016) 104–109.
[7] C.-L. Chen, Y. Zeng, Int. J. Refract. Metals Hard Mater. 60 (2016) 11–16.
[8] P.E. Lhuillier, T. Belhabib, P. Desgardin, B. Courtois, T. Sauvage, M.F. Barthe, A.L. Thomann, P. Brault, Y. Tessier, J. Nucl. Mater. 433 (2013) 305–313.
[9] M.H. Cui, Z.G. Wang, L.L. Pang, T.L. Shen, C.F. Yao, B.S. Li, J.Y. Li, X.Z. Cao, P. Zhang, J.R. Sun, Y.B. Zhu, Y.F. Li, Y.B. Sheng, Nucl. Instrum. Methods Phys. Res. B 307 (2013) 507–511.
[10] Xin Ou, Hong-Bo Zhou, Wolfgang Anwand, Reinhard Kögler, Asta Richter, J. Appl. Phys. 115 (2014) 123521–123521-7.
[11] C.L. Dube, P.K. Kulriya, D. Dutta, P.K. Pujari, Y. Patil, M. Mehta, P. Patel, S.S. Khirwadkar, J. Nucl. Mater. 467 (2015) 406–412.
[12] R. Kögler, W. Anwand, A. Richter, M. Butterling, Xin Ou, A. Wagner, C.-L. Chen, J. Nucl. Mater. 427 (2012) 133–139.
[13] C.-L. Chen, A. Richter, R. Kögler, J. Alloys Compd. 586 (2014) S173–S179.
[14] H. Trinkaus, B.N. Singh, J. Nucl. Mater. 323 (2003) 229.
[15] W.D. Wilson, C.L. Bisson, M.I. Baskes, Phys. Rev. B 24 (1981) 5616.
[16] J. Boisse, A. De Backer, C. Domain, C.S. Becquart, J. Mater. Res. 29 (2014) 2374–2386.
[17] Dimitrios Maroudas, Sophie Blondel, Lin Hu, Karl D. Hammond, Brian D. Wirth, J. Phys. Condens. Matter 28 (2016) 064004.
[18] Danny Perez, Luis Sandoval, Sophie Blondel, Brian D. Wirth, Blas P. Uberuaga, Arthur F. Voter, The Mobility of Small Vacancy/helium Complexes in Tungsten and its Impact on Retention in Fusion-relevant Conditions Preprint, 2017.
[19] J.F. Ziegler, J.P. Biersack, M.D. Ziegler, SRIM - the Stopping and Range of Ions in Matter, 2008. SRIM Co. ISBN 0-9654207-1-X.
[20] H. Surbeck, Helvetica Phys. Acta 50 (1977) 705–710.
[21] W. Anwand, H.-R. Kissener, G. Brauer, Acta Phys. Pol. A 88 (1995) 7–11.
[22] W. Anwand, G. Brauer, M. Butterling, H.-R. Kissener, A. Wagner, Defect Diffusion Forum 331 (2012) 25–41.
[23] W.C. Oliver, G.M. Pharr, J. Mater. Res. 7 (1992) 1564–1580.
[24] A. Richter, R. Smith, Encyclopedia of nanoscience and nanotechnology, Am. Sci. Publ. 17 (2011) 375–438.
[25] B. Wolf, A. Richter, New J. Phys. 5 (2003) 15.1–15.17.
[26] W.D. Nix, H. Gao, J. Mech. Phys. Solids 46 (1998) 411–425.
[27] P. Hosemann, D. Kiener, Y. Wang, S.A. Maloy, J. Nucl. Mater. 425 (2012) 136–139.
[28] J.V. Olsen, P. Kirkegaard, N.J. Pedersen, M. Eldrup, M. Phys. Stat. Sol. (c) 4 (2007) 4004–4006. www.palsfit.dk.
[29] Z. Shengyun, X. Yongjun, W. Zhiqiang, Z. Yongnan, Z. Dongmei, D. Enpeng, Y. Daqing, M. Fukuda, M. Mihara, K. Matsuta, T. Minamisono, J. Nucl. Mater. 343 (2005) 330–332.
[30] T. Troev, E. Popov, N. Nankov, T. Yoshiie, J. Phys. Conf. Ser. 207 (2010) 012033.
[31] R. Rajaraman, G. Amarendra, C.S. Sundar, Phys. Stat. Sol. 6 (2009) 2285–2290.
[32] R. Kögler, W. Anwand, A. Richter, M. Butterling, A. Mücklich, Xin Ou, H. Reuther, C.-L. Chen, Investigation of dual beam implanted oxide dispersed strengthened (ODS) alloy by positron annihilation spectroscopy (PAS), Trans Tech Publications, Switzerland, Near surface depth profiling of solids by mono-energetic positrons, in: B.N. Ganguly, G. Brauer (Eds.), Defect and Diffusion Forum, vol. 331, 2012, pp. 149–163.
[33] R. Zaleski, K. Zaleski, M. Gorgol, M. Wiertel, Appl. Phys. A 120 (2015) 551–559.
[34] A. Hirata, T. Fujita, Y.R. Wen, J.H. Schneibel, C.T. Liu, M.W. Chen, Nat. Mater. Lett. 10 (2011) 922–926.
[35] S.K. James, L. Gibson, S.G. Roberts, D.E.J. Armstrong, Mater. Sci. Eng. A 625 (2015) 380–384.